water

MDPI

Article

Sheet-like Skeleton Carbon Derived from Shaddock Peels with Hierarchically Porous Structures for Ultra-Fast Removal of Methylene Blue

Panlong Dong [1], Hailin Liu [1], Shengrui Xu [1,*], Changpo Chen [1], Suling Feng [1] and Anying Long [2,*]

[1] Key Laboratory of Green Chemical Media and Reactions, Ministry of Education, Collaborative Innovation Center of Henan Province for Green Manufacturing of Fine Chemicals, School of Chemistry and Chemical Engineering, Henan Normal University, Xinxiang 453007, China; pldong2000@163.com (P.D.); LiuHailin20211001@163.com (H.L.); andychen2005@163.com (C.C.); slfeng@htu.cn (S.F.)

[2] 113 Geological Brigade, Guizhou Bureau of Geology and Mineral Resources, Liupanshui 553000, China

* Correspondence: xushengrui@126.com (S.X.); longying031042@163.com (A.L.)

Abstract: To remove the pollutant methylene blue (MB) from water, a sheet-like skeleton carbon derived from shaddock peels (SPACs) was prepared by NaOH activation followed by a calcination procedure under nitrogen protection in this study. Characterization results demonstrated that the as-prepared SPACs displayed a hierarchically porous structure assembled with a thin sheet-like carbon layer, and the surface area of SPAC-8 (activated by 8 g NaOH) was up to 782.2 m^2/g. The as-prepared carbon material presented an ultra-fast and efficient adsorption capacity towards MB due to its macro-mesoporous structure, high surface area, and abundant functional groups. SPAC-8 showed ultrafast and efficient removal capacity for MB dye. Adsorption equilibrium was reached within 1 min with a removal efficiency of 99.6% at an initial concentration of 100 mg/g under batch adsorption model conditions. The maximum adsorption capacity for MB was up to 432.5 mg/g. A pseudo-second-order kinetic model and a Langmuir isotherm model described the adsorption process well, which suggested that adsorption rate depended on chemisorption and the adsorption process was controlled by a monolayer adsorption, respectively. Furthermore, column adsorption experiments showed that 96.58% of MB was removed after passing through a SPAC-8 packed column with a flow rate of 20 mL/min, initial concentration of 50 mg/L, and adsorbent dosage of 5 mg. The as-prepared adsorbent displays potential value in practical applications for dye removal due to its ultrafast and efficient adsorption capacity.

Keywords: shaddock peel-derived carbon; sheet-like skeleton; adsorbent; methylene blue; removal

Citation: Dong, P.; Liu, H.; Xu, S.; Chen, C.; Feng, S.; Long, A. Sheet-like Skeleton Carbon Derived from Shaddock Peels with Hierarchically Porous Structures for Ultra-Fast Removal of Methylene Blue. *Water* **2021**, *13*, 2554. https://doi.org/10.3390/w13182554

Academic Editor: Layla Ben Ayed

Received: 19 August 2021
Accepted: 14 September 2021
Published: 17 September 2021

1. Introduction

The rapid development of synthetic dyes has efficiently promoted the industrial growth in applications such as the leather, paint, textile and other industries. However, the usage of large amounts of dyes has resulted in severe environmental issues due to the disposal of dye-containing wastewaters in aqueous systems [1–3]. Wastewater containing synthetic dyes reduces light penetration in receiving water bodies and thus affects the photosynthetic activities of aquatic flora, destroying the aqueous system, thereby badly affecting the food sources of aquatic organisms [4]. For instance, the presence of malachite green in water can cause breathing problems and swimming difficulties for fish [5]. Various techniques including adsorption, membrane separation [6], biological treatment [7], and catalytic degradation [8,9] have been investigated to remove dye pollutants from water bodies. Owing to its outstanding advantages of low cost, effectiveness and operability, the adsorption technique has been extensively used for pollutant removal [10]. Undoubtedly, preparation of a high-performance material is the key to efficient removal of dyes.

Various materials such as activated carbon [11], nano-composites [12], polymers [13], graphene-based composites [14], etc. have been used as adsorbents for pollutant removal.

Activated carbon-based adsorbents present unique advantages for pollutant adsorption due to their high adsorption capacity, renewability and low cost. Furthermore, activated carbon is easy to obtain, and can be derived from agricultural waste. [1,15]. Yu et al. [16] prepared a honeycomb-like activated carbon from popcorn following with NaOH activation. The prepared activated carbon presented a high adsorption capacity for Rhodamine B dye with an equilibrium time of 12 h. Auta et al. [17] investigated the removal capacity of methylene blue (MB) and acid blue 29 (AB29) dyes by waste tea-derived activated carbon. Their results showed that waste tea activated carbon presented a maximum adsorption capacity of 554.30 and 453.12 mg/g for MB and AB29 with an equilibrium time of about 12 h. Gupta et al. [18] prepared an activated carbon material from lignocellulosic agro-waste, and investigated its adsorption capacity towards dyes. The results illustrated that the adsorption reached equilibrium within 20 min at an initial concentration of 50 mg/L, and the maximum adsorption capacity for MB was 537.6 mg/g.

Numerous works towards dye removal by biomass derived activated carbon materials have been studied, and an efficient dye adsorption capacity demonstrated. However, previous studies on dye removal by biomass-derived carbon materials suffered from slow uptake rates. Rapid adsorption of dye pollutants can greatly reduce the time consumed and labor costs in practical applications. Some researchers have been concerned with improving the rate of pollutant removal. For example, Lin et al. [19] fabricated a hollow poly-dopamine nanomaterial for rapid removal of dye pollutants from water. The results demonstrated that more than 98% of MB dye was removed by the prepared adsorbent in 20 s. Gissawong et al. [20] investigated the adsorption capacity of sponge embedded with deep eutectic solvent towards dye and organophosphorus pesticide pollutants with a vortex-assistant model, and reported a rapid pollutant removal rate with removal efficiency higher than 75% in 30 s. Nevertheless, the adsorbents for rapid pollutant removal from water are very much limited to advanced materials, including porous polymers, mesoporous silica, MOF-based adsorbents, etc., which would result in higher use cost than the use of biomass-derived carbon materials as adsorbents in practical applications.

Herein, we demonstrated an approach to prepare shaddock peel-derived activated carbon materials (SPACs) composed of a sheet-like skeleton possessing a hierarchical pore structure by sodium hydroxide activation during a calcination process under nitrogen protection. Methylene blue (MB) was chosen as model dye pollutant to evaluate the adsorption capacity of the as-prepared adsorbents both in batch and column models. The as-prepared SPACs adsorbents exhibited an ultrafast and efficient adsorption capacity towards MB dye from aqueous solution. This study provides an efficient approach to the removal of dye pollutants from water.

2. Experimental

2.1. Materials and Reagents

Shaddock peels used as our raw material were collected from a local market. Chemical reagents including methylene blue (MB), hydrochloric acid (HCl) and sodium hydroxide (NaOH) were purchased from Sinopharm Chemical Reagent Co., Ltd. (Beijing, China). All the solutions used in the experiments were prepared with deionized water.

2.2. Preparation of SPACs Adsorbents

The SPACs adsorbents were prepared by a carbonization procedure under nitrogen followed by NaOH activation. Firstly, shaddock peels were cut into small pieces after removing the outer yellow layer. Then the shaddock peel pieces were cleaned with deionized water and put into a freeze drier for 2 days. After drying by the freeze-drying method, the shaddock peel pieces were crushed into a powder using a grinder. Ten g of shaddock peel powder was further mixed with NaOH and 20 mL deionized water by stirring thoroughly for 2 h, and then put into a freeze-drier for 2 days. The weights of NaOH added were set at 0, 2, 4, 6 and 8 g and the resulting activated carbons were denoted as SPAC-0, SPAC-2, SPAC-4, SPAC-6 and SPAC-8, respectively. The dried mixture was transferred into a hori-

zontal quartz tube furnace (BTF-1200CC-S, Anhui BEQ Equipment Technology Co., Ltd., Hefei, China), which had been purged with nitrogen for 1 h. The calcination procedure was carried out by heating from 30 to 800 °C with a heating rate of 2 °C/min, and then holding at 800 °C for 2 h under a nitrogen atmosphere. After cooling to room temperature, the obtained activated carbon materials were rinsed with 0.1 M HCl solution and deionized water to neutrality. Finally, the SPACs adsorbents with hierarchical pore structures were obtained after drying in a vacuum oven overnight at 80 °C.

2.3. Characterizations of Adsorbents

The morphology of the as-prepared SPACs adsorbents was characterized by scanning electron microscopy (SEM, SU8010, HITACHI, Tokyo, Japan) and transmission electron microscopy (TEM, JEM-2100, JEOL, Tokyo, Japan). The BET surface area and average pore diameter of as-prepared adsorbents were analyzed by a nitrogen adsorption/desorption apparatus (Micromeritics ASAP 2020 M, Atlanta, GA, USA). The surface chemical state was investigated using X-ray photoelectron spectroscopy (XPS, VG Multilab 2000 X spectrometer, Thermo Fisher Scientific, Waltham, MA, USA). Raman spectra were obtained by using a LabRam-1B Raman system (HORIBA Scientific, Tokyo, Japan) equipped with a 532 nm excitation laser.

2.4. Adsorption Experiments

To better demonstrate the adsorption capacity of as-prepared SPACs adsorbents towards MB dye, both batch and column adsorption model were investigated in this experiment.

- *Batch adsorption*. Typically, 10 mg of SPACs adsorbents was placed in a glass vial (20 mL) which containing 10 mL MB solution with a fixed initial concentration of 100 mg/g. Then, the glass vial was sealed and shaken on a SHA-B shaker (Changzhou Tianrui Instrument Co. Ltd., Changzhou, China) with a speed of 200 rpm. After adsorption for a certain time, the solution was filtered by using a syringe-driven filter, which was equipped with a 0.45 μm filter membrane. The concentration of MB in filtrate was determined using a UV-vis spectrophotometer (722N, Shanghai Jinghua Instrument Co. Ltd., Shanghai, China) at a wavelength of 662 nm. The amounts of MB adsorbed per mass of SPACs (q, mg/g) and MB removal rate (R, %) were calculated by means of the following Equations (1) and (2), respectively:

$$q = \frac{(C_0 - C_e)V}{m} \quad (1)$$

$$R = \frac{C_0 - C_e}{C_0} \times 100\% \quad (2)$$

  where, C_0 (mg/g) is the initial concentration of MB, and C_e (mg/g) represents the equilibrium concentration, respectively; V (mL) is the solution volume; m (g) denotes the mass of adsorbent.
- *Column adsorption*. The column adsorption procedure was performed by using a solid phase extraction device (Shanghai Lichen Instrument Technology Co., Ltd., Shanghai, China) and plastic columns with inner diameter of 5.6 mm and length of 66.3 mm. An AP-02B vacuum pump (Tianjin Automatic Science Instrument Co., Ltd., Tianjin, China) was used to maintain the volumetric flow rate. Briefly, 5 mg of adsorbents were filled to plastic columns with heights of 6 mm, and MB solutions with initial concentration of 10–200 mg/L were passed through the column at a volumetric flow rate of 20 mL/min. The concentrations of solutions collected after through the column were analyzed by using UV-vis spectrophotometer at a wavelength of 662 nm. MB removal rate (R, %) were calculated using abovementioned Equation (2).

3. Results and Discussion

3.1. Characterizations of As-Prepared Adsorbents

The surface morphology and size of as-prepared adsorbents (SPAC-0, SPAC-2, SPAC-4, and SPAC-8) were investigated by SEM. Figure 1a illustrates the irregular block texture without apparent porous structure of the SPAC adsorbents. After chemical activation by NaOH, SPACs preserves a honeycomb-like structure with abundant pores (Figure 1b,c). SPAC-4 presents more abundant pores than SPAC-2 with increasing amount of NaOH addition from 2 g to 4 g. Furthermore, following activation by 8 g NaOH, SPAC-8 exhibits a thin sheet-like skeleton structure assembled together to form hierarchical porous textures (Figure 1d). TEM characterization demonstrates that SPAC-8 presents a morphology similar to a sheet-like structure with distributed mesopores (Figure 1e,f). Porous and thin sheet-like structures of SPACs were obtained with the carbonization procedure after NaOH activation. The chemical activation mechanism of NaOH can be depicted in Equations (3)–(6) [21–24]. Firstly, Na_2CO_3 and H_2 components are generated by reaction of NaOH and C. Then, part of the Na_2CO_3 reacts with C to produce CO, and the other part decomposes into Na_2O and CO_2 components under the employed high temperature conditions. Meanwhile, Na_2O can also react with C to create CO compounds. In summary, the activation process with NaOH will result in the release of plenty of reaction gases containing CO_2, CO, and H_2 at high temperature in the nitrogen atmosphere. The gas release and carbon atoms elimination leave numerous vacancies in the materials, which result in the observed hierarchical porous textures [16,25,26].

$$6NaOH + 2C \rightarrow 2Na + 3H_2 + 2Na_2CO_3 \quad (3)$$

$$Na_2CO_3 + 2C \rightarrow 2Na + 3CO \quad (4)$$

$$Na_2CO_3 \rightarrow Na_2O + CO_2 \quad (5)$$

$$Na_2O + C \rightarrow 2Na + CO \quad (6)$$

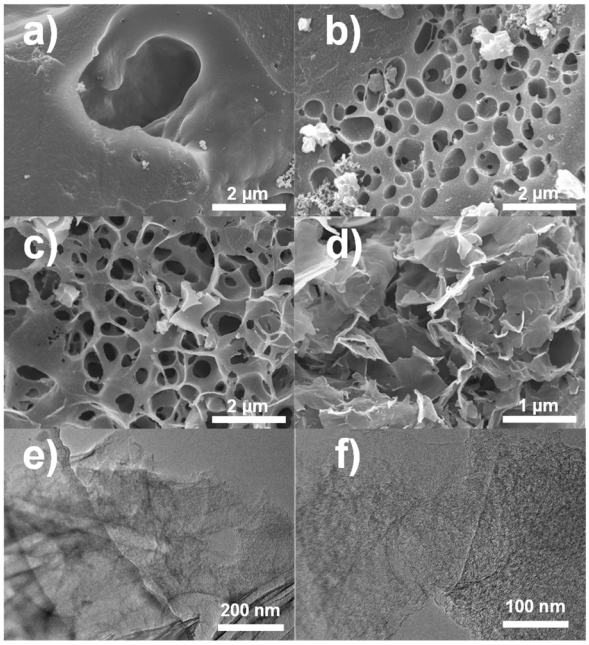

Figure 1. SEM images of SPAC-0 (**a**), SPAC-2 (**b**), SPAC-4 (**c**), SPAC-8 (**d**), and TEM images of SPAC-8 (**e**,**f**).

The N2 adsorption-desorption isotherms and pore size distributions of SPAC-0, SPAC-4 and SPAC-8 are shown in Figure 2. The N2 adsorption-desorption isotherms show a typical type IV isotherm and H3 hysteresis loop for SPAC-0 and SPAC-8 (Figure 2a). SPAC-4 presents a type III isotherm with H3 hysteresis loop (appearing in the range from

0.4 to 1.0 of relative pressure). The increase of N_2 adsorption in the relative pressure range of 0–0.9 and distinct hysteresis loop is correlated to the abundant mesoporous and macroporous structures [27,28]. The steep increase of N_2 adsorption in the relative pressure range of 0.9–1.0 indicated that macropore structures were generated for SPAC-4 and SPAC-8 [29]. The BET specific surface areas of prepared SPAC-0, SPAC-4 and SPAC-8 materials were calculated to be 108.7, 490.5 and 782.2 m^2/g, respectively. In comparison to SPAC-0, the BET specific surface area of SPAC-8 increased dramatically due to chemical activation by NaOH, which promoted the formation of mesoporous and macroporous structures on SPACs during the thermal decomposition process [30,31]. The mesoporous and macroporous textures of the prepared SPACs adsorbents are further verified by the pore size distribution, which is calculated from the corresponding density functional theory. It can be observed from Figure 2b that the pores size of SPAC-4 and SPAC-8 has a wide range of size distribution from 17–50 nm for mesopores and 50–1200 nm for macropores. However, there are only slight mesopores distribution and no obvious macropores texture for SPAC-0 adsorbent, which is in good accordance with the SEM results (Figure 1a).

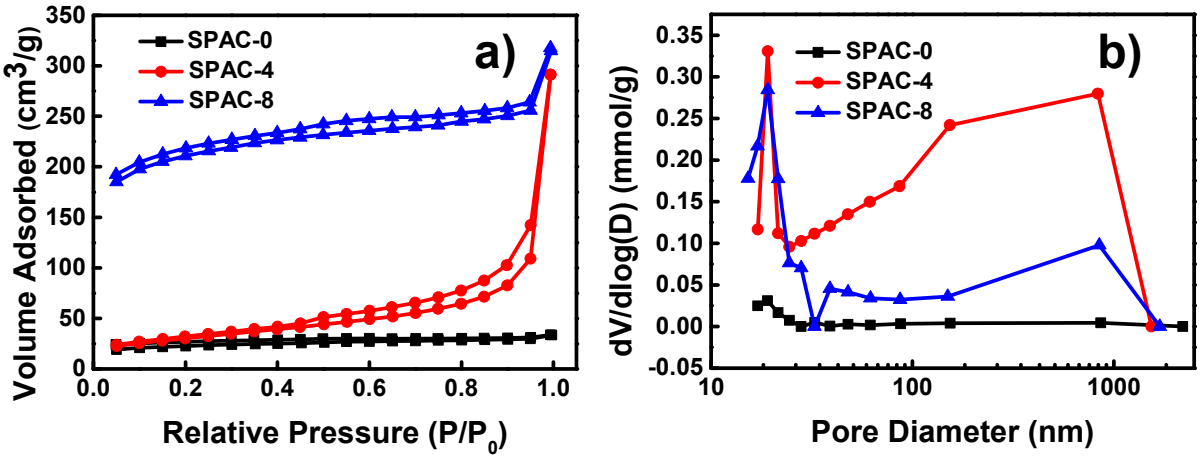

Figure 2. N_2 adsorption-desorption isotherms (**a**) and pore size distributions (**b**) of SPAC-0, SPAC-4 and SPAC-8.

Raman spectra of the prepared SPACs adsorbents are depicted in Figure 3a. As shown in Figure 3a, all SPACs studied exhibit two typical broad peaks of amorphous biomass carbon at ~1350 and 1590 cm^{-1}, which are corresponding to the disorder-induced D-band and in-plane vibrational G-band, respectively. The intensity ratio of D and G band (I_D/I_G), which is used to evaluate the defects of carbon materials, is calculated to be about 0.98 for all the prepared SPACs, indicating that the prepared SPACs exhibit disordered structures because of gas release during the carbonization procedure.

The chemical states and functional groups of as-prepared SPAC-8 adsorbent was investigated by XPS analysis. As shown in Figure 3b, two kinds of elements including C and O were detected for SPAC-8 in the survey XPS spectra with the atomic C of 94.14% and atomic O of 5.44%, respectively. The high-resolution XPS spectra of C 1s (Figure 3c) can be deconvoluted into four peaks, corresponding to sp^2 C (284.8 eV), C-O (286.2 eV), C=O (288.3) and O-C=O (290.6 eV), respectively [32–34]. The deconvolution of O 1s presents three peaks at 531.1, 532.3 and 533.3 eV, which are attributed to C=O, C-O and O-C=O bond, following the consistent consequences with de-convoluted results of C 1s XPS spectra (Figure 3d). Abundant oxygen-containing groups obtained on adsorbents would easily promote the formation of hydrogen-bonding between adsorbents and adsorbates, which can accelerate the adsorption capacity [35].

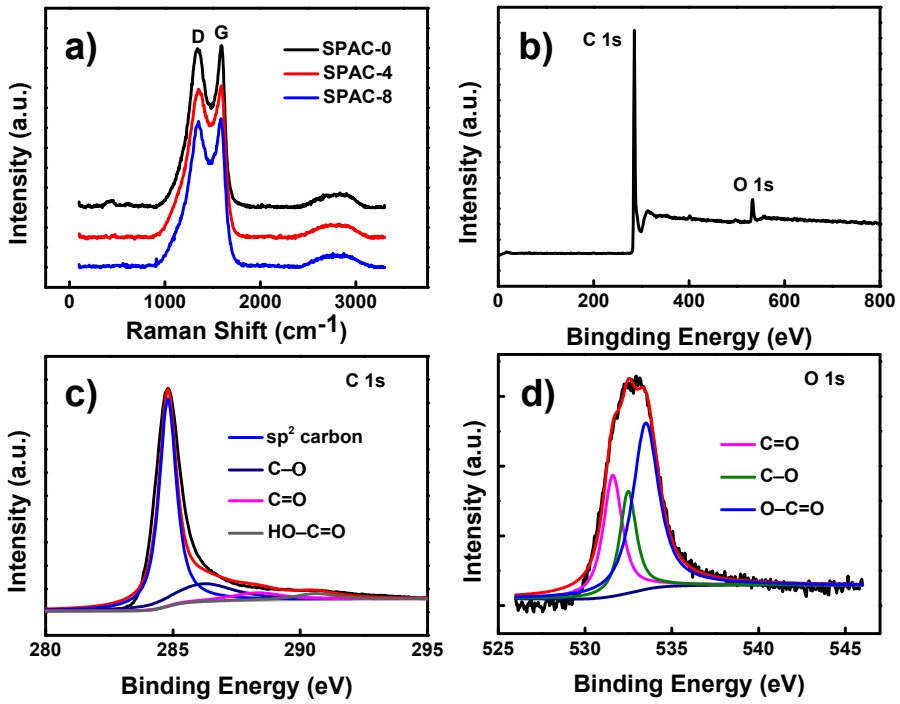

Figure 3. Raman spectra of SPAC-0, SPAC-4 and SPAC-8 (**a**), survey XPS spectra of SPAC-8 (**b**), and high-resolution C 1s spectra (**c**), high-resolution O 1s spectra (**d**) of SPAC-8.

3.2. Adsorption Performance of MB with Batch Model

3.2.1. Effect of Contact Time

A short contact time on equilibrium adsorption plays an important role in the rapid removal of pollutants by an adsorbent [36]. Figure 4a shows the effect of contact time on the removal capacity of prepared SPACs adsorbents towards MB dye. It can be seen that the removal efficiencies of SPACs adsorbents towards MB dye increase with the increase of contact time firstly, and then reach a stable value with further prolonged time. Predictably, the SPACs adsorbents after NaOH activation present much higher adsorption capacity than that without NaOH activation (SPAC-0) towards MB dye. Approximately 100% of MB was adsorbed by SPAC-2, SPAC-4, SPAC-6 and SPAC-8 adsorbents after adsorption equilibrium with initial concentration of 100 mg/L. It is worth noting that SPAC-8 demonstrates quite fast adsorption rate towards MB dye. The removal efficiency of SPAC-8 can reach 99.6% within 1 min. The ultra-fast adsorption rate towards MB can be attributed to the high surface area and the hierarchical porous structures of the SPACs.

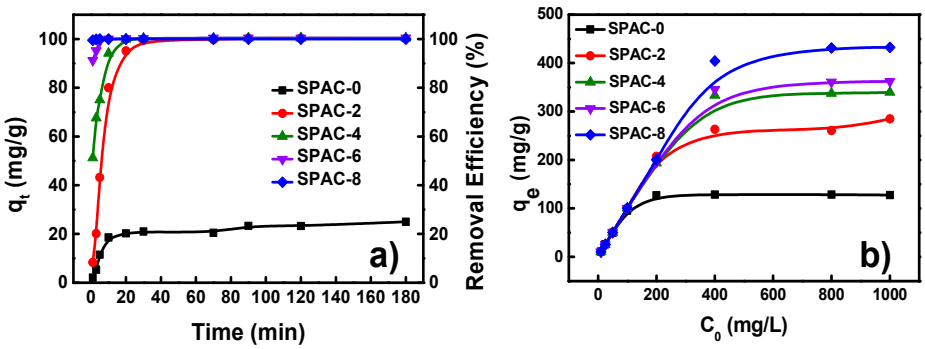

Figure 4. Effect of (**a**) contact time and (**b**) initial concentration on removal capacities of SPACs towards MB.

3.2.2. Effect of Initial Concentration

Figure 4b reveals the effect of initial concentration on adsorption efficiency towards MB by using SPACs adsorbents with a contact time of 30 min. Obviously, the adsorption efficiency of SPACs adsorbents increases with the increase in MB concentration from 10 to 400 mg/L, and then reaches adsorption equilibrium with further increase of the MB concentration. The adsorption capacity of SPACs presents a distinct increase with increasing addition amounts of NaOH from 0 to 8 g due to its chemical activation in the carbonization process. The maximum adsorption capacity of SPAC-8 is 432.5 mg/g, which is far higher than that of SPAC-0 (128.6 mg/L).

3.3. Adsorption Kinetics

To evaluate the adsorption rate, the adsorption kinetics of as-prepared SPACs adsorbents towards MB were investigated using both pseudo-first-order and pseudo-second-order kinetic models. The pseudo-first-order kinetic assumes that mass transfer and diffusion of adsorbates to adsorbents control the adsorption process, whereas chemisorption mainly determines the adsorption process for pseudo-second-order kinetic model [37,38]. The adsorption kinetic data was fitted using pseudo-first-order model (Equation (7)) and pseudo-second-order model (Equation (8)) in the following equations:

$$ln(q_e - q_t) = lnq_e - k_1 t \quad (7)$$

$$\frac{t}{q_t} = \frac{1}{k_2 q_e^2} + \frac{t}{q_e} \quad (8)$$

where q_e and q_t are the amounts of adsorbed dye (mg/g) at equilibrium and at time t (min), respectively; k_1 (/min) and k_2 (g/mg·min) are the pseudo-first and pseudo second order rate constants, respectively.

The fitted curves of experimental data are given in Figures S1 and S2, and kinetic model parameters as well as correlation coefficients are summarized in Table 1. As shown in Figures S1 and S2 and Table 1, the correlation coefficients (R^2) of the pseudo-second-order kinetic model present greater than 0.99 for all the adsorbents, which are higher than those of pseudo-first-order model. Furthermore, the calculated values of the equilibrium adsorption capacity ($q_{e,cal}$) from pseudo-second-order show perfect agreement with the experimental values ($q_{e,exp}$). These results demonstrate that chemisorption is the main factor to control the adsorption rate rather than diffusion and mass transfer.

Table 1. Kinetic model parameters and correlation coefficients (R^2) for the adsorption of MB onto SPACs.

Adsorbents	$q_{e,exp}$ (mg/g)	Pseudo-First-Order			Pseudo-Second-Order		
		$q_{e,cal}$ (mg/g)	k_1 (/min)	R^2	$q_{e,cal}$ (mg/g)	K_2 (g/mg·min)	R^2
SPAC-0	23.3	28.1	0.1455	0.9844	24.8	0.0077	0.9923
SPAC-2	100.3	78.9	0.1747	0.9607	103.1	0.0026	0.9946
SPAC-4	100.4	123.9	0.2521	0.9598	101.0	0.0078	0.9998
SPAC-6	100.4	106.6	2.482	0.8765	101.0	0.0754	0.9999
SPAC-8	100.2	148.0	4.001	0.9917	100.0	0.2000	0.9999

3.4. Adsorption Isotherms

To investigate the adsorption mechanism of the MB dye molecules on the surface of SPACs adsorbents, the adsorption isotherms was fitted according to Langmuir and Freundlich isotherm models, respectively. Wherein the Langmuir isotherm applies for a homogeneous adsorption surface, the Freundlich isotherm is applied to predict adsorption over heterogeneous surfaces [39,40]. The Langmuir and Freundlich isotherm model can be expressed as Equations (9) and (10):

$$\frac{C_e}{q_e} = \frac{C_e}{q_m} + \frac{1}{k_L q_m} \quad (9)$$

$$lnq_e = lnk_F + \frac{1}{n_F} lnC_e \quad (10)$$

where C_e is the equilibrium concentration (mg/L) and qm represents the maximum adsorption amounts on monolayer coverage (mg/L). k_L is a constant related to the free adsorption energy (L/mg). k_F and n_F represent the Freundlich isotherm constant and adsorption intensity, respectively.

The fitting curves of the Langmuir and Freundlich model are shown in Figure S3, and the adsorption isotherm parameters and correlation coefficients (R^2) for the adsorption of MB were summarized in Table 2. Comparing the correlation coefficients of the Langmuir and Freundlich fitting curves, the results suggest that the Langmuir isotherm model can describe the adsorption process towards MB for the as-prepared adsorbents better than the Freundlich isotherm model. It can be observed that adsorption process is mainly controlled by a monolayer adsorption process.

Table 2. Adsorption isotherm parameters and correlation coefficients (R^2) for the adsorption of MB onto SPACs.

Adsorbents	$q_{m,exp}$ (mg/g)	Langmuir			Freundlich		
		q_m (mg/g)	k_L (L/mg)	R^2	n_f	K_f	R^2
SPAC-0	128.7	127.6	0.632	0.9999	9.15	67.5	0.8281
SPAC-2	278.7	274.7	0.569	0.9972	7.63	226.6	0.7420
SPAC-4	339.6	337.8	0.643	0.9997	8.43	169.6	0.7404
SPAC-6	362.2	359.7	0.381	0.9994	8.31	180.5	0.7938
SPAC-8	432.5	434.8	0.228	0.9993	13.6	429.9	0.8199

3.5. Comparisons of Adsorption Capacities with Other Adsorbents

To evaluate the adsorption capacity of as-prepared adsorbent towards MB, comparisons of adsorption capacities with various adsorbents are list in Table 3. The maximum adsorption amount of as-prepared SPAC-8 adsorbent is 432.5 mg/g, which performs an adsorption capacity comparable to other adsorbents. What is noteworthy is that the adsorption time of SPAC-8 towards MB is lower than 1 min to achieve equilibrium, which presents much higher adsorption rate than other adsorbents. The ultra-fast adsorption rate provides a potential application for MB removal with column adsorption in practice.

Table 3. Comparisons of adsorption capacities towards MB with other adsorbents.

Adsorbents	Adsorption Capacity (mg/g)	Adsorption Time (min)	Reference
Magnetic chitosan/graphene oxide	95.16	60	[41]
HKUST-1 modified cellulose/chitosan composite	526.3	900	[42]
Loofah fiber-graft-polyacrylic acid	302.4	3	[43]
Cellulose−clay nanocomposite hydrogels	782.9	20	[44]
Activated carbon derived from cashew nut shells	476	1440	[45]
Activated carbon derived from Malawian baobab fruit shells	334.45	60	[46]
Cellulose microfilament spheres	497.5	180	[47]
SPAC-8	432.5	≤1	This work

3.6. Reusability of SPAC-8

The regeneration and reusability of adsorbents play an important role in their potential practical applicability. After adsorption of MB by SPAC-8 adsorbent, desorption experiments were carried out by rinsing the MB adsorbed on the adsorbent with ethanol three times and with deionized water three times. Afterwards, the dried SPAC-8 adsorbent was used again for adsorbing MB to evaluate the reusability. In this work, the adsorption-desorption experiment was repeated for four cycles. As shown in Figure 5, the removal efficiency of SPAC-8 towards MB displays a gradually decreasing trend with increasing reuse times because of the decreased number of active sites [48,49]. It is worth mentioning

that even though the removal efficiency decreases when reusing the adsorbent, the removal efficiency of SPAC-8 can reach more than 80% after five regeneration cycles, which indicates that the prepared adsorbents possess good regenerability and reusability.

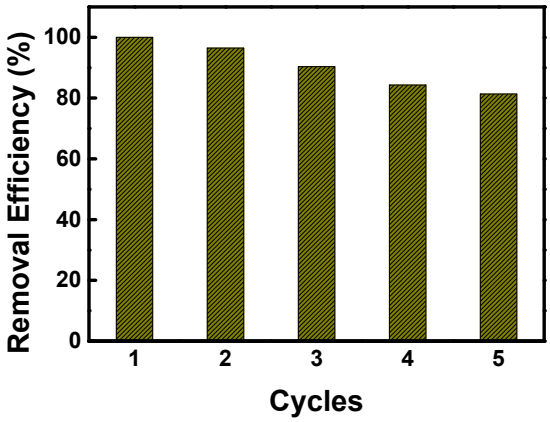

Figure 5. Reusability of SPAC-8 for the adsorption of MB.

3.7. Column Adsorption

To demonstrate the potential application of as-prepared adsorbents for MB removal in practice, column adsorption experiments of SPAC-8 adsorbent were performed in this work by using a solid phase extraction device. Firstly, the effect of flow velocity (10, 20, 30 and 40 mL/min) on MB removal capacity was evaluated with an initial MB concentration of 50 mg/L, solution volume of 10 mL and adsorbent dosage of 5 mg. As shown in Figure 6, approximately 100% of the MB is removed after passing through the SPAC-8 packed column with a flow velocity of 10 mL/min, and the solution becomes colorless. The removal efficiency towards MB decreases to 96.58% following the increase of the flow rate to 20 mL/min, and continues to decrease with further flow rate increases. The diminished removal capacity towards MB is ascribed to insufficient residence time of the solute in the column, which results in a short contact time between the MB and the adsorbent, and the solution is discharged from the column before reaching adsorption equilibrium [50,51].

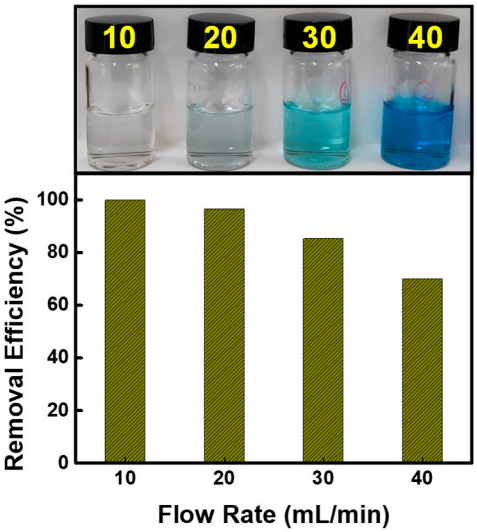

Figure 6. Effect of flow rate on MB removal efficiency for SPAC-8 with initial concentration of 50 mg/L, solution volume of 10 mL and adsorbent dosage of 5 mg.

Furthermore, the effect of MB initial concentration on the removal efficiency of the SPAC-8 adsorbent in a column adsorption model was investigated with a flow rate of

20 mL/min, solution volume of 10 mL and adsorbent dosage of 5 mg. As shown in Figure 7, the removal efficiency of SPAC-8 adsorbent is approximately 100% when the initial concentration of MB was is equal to or lesser than 25 mg/L, and the solution collected from column outlet turned completely colorless. The color change from blue to colorless with an initial concentration of 50 mg/L, solution volume of 10 mL, flow rate of 20 mL/min, and adsorbent dosage of 5 mg can be better visualized in the recorded Video S1. The removal efficiency displays a gradual decline with the increase of initial concentration of MB due to the adsorption capacity limitation of SPAC-8 and the restricted contact time between solute and adsorbents while MB solution passes though the packed column. The adsorbed amounts of SPAC-8 towards MB increases firstly with increasing initial concentration from 5 mg/L to 250 mg/L, and reaches a constant level with further extend initial concentration due to the limitation of maximum adsorption capacity. With the column adsorption model, the maximum adsorption capacity of SPAC-8 adsorbent is 401.1 mg/g towards MB dye, which is lower than the maximum adsorption capacity with the batch adsorption model. This phenomenon can be explained by an insufficient residence time of the solute in the column that leads to inadequate diffusion of the solute into the adsorbent pores [50].

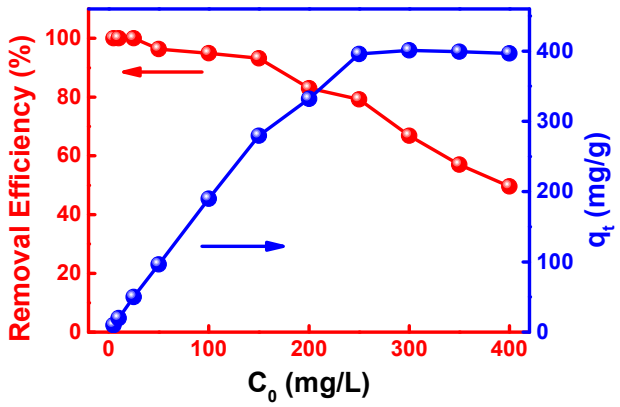

Figure 7. Effect of MB initial concentration on removal capacity for SPAC-8 with flow rate of 20 mL/min, solution volume of 10 mL and adsorbent dosage of 5 mg.

4. Conclusions

In summary, the carbon materials derived from shaddock peels were prepared by a calcination procedure under nitrogen protection after NaOH activation. The as-prepared carbon material displayed a macro-mesoporous hierarchical structure composed of a thin carbon layer. The high surface area and abundant functional groups make SPAC-8 exhibit an ultra-fast and efficient adsorption capacity towards MB, resulting in a maximum adsorption of 432.5 mg/g and short equilibrium time (within 1 min) at an initial concentration of 100 mg/L. Column adsorption also demonstrated the ultra-fast removal capacity of SPAC-8 towards MB. The excellent adsorption performance towards MB make SPACs good potential adsorbents for dye removal from wastewater.

Supplementary Materials: The following are available online at https://www.mdpi.com/article/10.3390/w13182554/s1, Figure S1: pseudo-first-order kinetic fitting curves, Figure S2: pseudo-second-order kinetic fitting curves, Figure S3: fitting curves for MB adsorption onto SPACs based on Langmuir (a) and Freundlich (b) isotherms, Video S1: recorded video of column adsorption towards MB.

Author Contributions: P.D.: investigation and writing draft preparation. H.L.: formal analysis and investigation. S.X.: conceptualization, methodology, and writing—review and editing. C.C.: writing—review and editing. S.F.: supervision. A.L.: resources and funding acquisition. All authors have read and agreed to the published version of the manuscript.

Funding: This work was financially supported by funding from the National Natural Science Foundation of China (21976052, 21777038, 21977025), Natural Science Foundation of Guizhou Province of China ([2019]1423), the Youth Science Foundation of Henan Normal University (20200183), and Henan Special Support for High-level Talents Central Plains Science and Technology Innovation Leading Talents (204200510006).

Institutional Review Board Statement: Not Applicable.

Informed Consent Statement: Not applicable.

Data Availability Statement: This study presents novel concepts and did not report any data.

Conflicts of Interest: The authors declare no conflict of interest.

References

1. Hassan, M.M.; Carr, C.M. Biomass-derived porous carbonaceous materials and their composites as adsorbents for cationic and anionic dyes: A review. *Chemosphere* **2021**, *265*, 129087. [CrossRef]
2. Silva, T.L.; Ronix, A.; Pezoti, O.; Souza, L.S.; Leandro, P.K.T.; Bedin, K.C.; Beltrame, K.K.; Cazetta, A.L.; Almeida, V.C. Mesoporous activated carbon from industrial laundry sewage sludge: Adsorption studies of reactive dye Remazol Brilliant Blue R. *Chem. Eng. J.* **2016**, *303*, 467–476. [CrossRef]
3. Li, D.; Chai, K.; Yao, X.; Zhou, L.; Wu, K.; Huang, Z.; Yan, J.; Qin, X.; Wei, W.; Ji, H. beta-Cyclodextrin functionalized SBA-15 via amide linkage as a super adsorbent for rapid removal of methyl blue. *J. Colloid Interf. Sci.* **2021**, *583*, 100–112. [CrossRef]
4. Ali, H. Biodegradation of Synthetic Dyes—A Review. *Water Air Soil Poll.* **2010**, *213*, 251–273. [CrossRef]
5. Tkaczyk, A.; Mitrowska, K.; Posyniak, A. Synthetic organic dyes as contaminants of the aquatic environment and their implications for ecosystems: A review. *Sci. Total Environ.* **2020**, *717*, 137222. [CrossRef] [PubMed]
6. Chen, W.; Mo, J.; Du, X.; Zhang, Z.; Zhang, W. Biomimetic dynamic membrane for aquatic dye removal. *Water Res.* **2019**, *151*, 243–251. [CrossRef]
7. Catto, C.; Sanmartin, P.; Gulotta, D.; Troiano, F.; Cappitelli, F. Bioremoval of graffiti using novel commercial strains of bacteria. *Sci. Total Environ.* **2021**, *756*, 144075. [CrossRef]
8. Rachna; Rani, M.; Shanker, U. Synergistic effects of zinc oxide coupled copper hexacyanoferrate nanocomposite: Robust visible-light driven dye degradation. *J. Colloid Interf. Sci.* **2021**, *584*, 67–79. [CrossRef]
9. Jia, Y.; Liu, P.; Wang, Q.; Wu, Y.; Cao, D.; Qiao, Q.A. Construction of Bi2S3-BiOBr nanosheets on TiO_2 NTA as the effective photocatalysts: Pollutant removal, photoelectric conversion and hydrogen generation. *J. Colloid Interf. Sci.* **2021**, *585*, 459–469. [CrossRef]
10. Zhou, Y.; Lu, J.; Zhou, Y.; Liu, Y. Recent advances for dyes removal using novel adsorbents: A review. *Environ. Pollut.* **2019**, *252*, 352–365. [CrossRef] [PubMed]
11. Machado, F.M.; Bergmann, C.P.; Fernandes, T.H.M.; Lima, E.C.; Royer, B.; Calvete, T.; Fagan, S.B. Adsorption of Reactive Red M-2BE dye from water solutions by multi-walled carbon nanotubes and activated carbon. *J. Hazard. Mater.* **2011**, *192*, 1122–1131. [CrossRef]
12. Kim, T.S.; Song, H.J.; Dar, M.A.; Lee, H.J.; Kim, D.W. Fast adsorption kinetics of highly dispersed ultrafine nickel/carbon nanoparticles for organic dye removal. *Appl. Surf. Sci.* **2018**, *439*, 364–370. [CrossRef]
13. Nawaz, H.; Umar, M.; Ullah, A.; Razzaq, H.; Zia, K.M.; Liu, X. Polyvinylidene fluoride nanocomposite super hydrophilic membrane integrated with Polyaniline-Graphene oxide nano fillers for treatment of textile effluents. *J. Hazard. Mater.* **2021**, *403*, 123587. [CrossRef] [PubMed]
14. Manabe, S.; Kiliyankil, V.A.; Takiguchi, S.; Kumashiro, T.; Fugetsu, B.; Sakata, I. Graphene nanosheets homogeneously incorporated in polyurethane sponge for the elimination of water-soluble organic dyes. *J. Colloid Interf. Sci.* **2021**, *584*, 816–826. [CrossRef] [PubMed]
15. Godiya, C.B.; Ruotolo, L.A.M.; Cai, W. Functional biobased hydrogels for the removal of aqueous hazardous pollutants: Current status, challenges, and future perspectives. *J. Mater. Chem. A* **2020**, *8*, 21585–21612. [CrossRef]
16. Yu, Y.; Qiao, N.; Wang, D.; Zhu, Q.; Fu, F.; Cao, R.; Wang, R.; Liu, W.; Xu, B. Fluffy honeycomb-like activated carbon from popcorn with high surface area and well-developed porosity for ultra-high efficiency adsorption of organic dyes. *Bioresour. Technol.* **2019**, *285*, 121340. [CrossRef] [PubMed]
17. Auta, M.; Hameed, B.H. Optimized waste tea activated carbon for adsorption of Methylene Blue and Acid Blue 29 dyes using response surface methodology. *Chem. Eng. J.* **2011**, *175*, 233–243. [CrossRef]
18. Gupta, K.; Khatri, O.P. Fast and efficient adsorptive removal of organic dyes and active pharmaceutical ingredient by microporous carbon: Effect of molecular size and charge. *Chem. Eng. J.* **2019**, *378*, 122218. [CrossRef]
19. Lin, J.; Wang, H.; Ren, E.; Song, Q.; Lan, J. Stomatocyte-like hollow polydopamine nanoparticles for rapid removal of water-soluble dyes from water. *Chem. Commun.* **2019**, *55*, 8162–8165. [CrossRef] [PubMed]
20. Gissawong, N.; Mukdasai, S.; Boonchiangma, S.; Sansuk, S.; Srijaranai, S. A rapid and simple method for the removal of dyes and organophosphorus pesticides from water and soil samples using deep eutectic solvent embedded sponge. *Chemosphere* **2020**, *260*, 127590. [CrossRef]

21. Wang, Y.; Qu, Q.; Gao, S.; Tang, G.; Huang, C. Biomass derived carbon as binder-free electrode materials for supercapacitors. *Carbon* **2019**, *155*, 706–726. [CrossRef]
22. Doczekalska, B.; Bartkowiak, M.; Waliszewska, B.; Orszulak, G.; Cerazy-Waliszewska, J.; Pniewski, T. Characterization of chemically activated carbons prepared from miscanthus and switchgrass biomass. *Materials* **2020**, *13*, 1654. [CrossRef]
23. Alcañiz-Monge, J.; Illán-Gómez, M.J. Insight into hydroxides-activated coals: Chemical or physical activation. *J. Colloid Interf. Sci.* **2008**, *318*, 35–41. [CrossRef] [PubMed]
24. Lillo-Ródenas, M.A.; Juan-Juan, J.; Cazorla-Amorós, D.; Linares-Solano, A. About reactions occurring during chemical activation with hydroxides. *Carbon* **2004**, *42*, 1371–1375. [CrossRef]
25. Lee, D.; Cho, Y.G.; Song, H.K.; Chun, S.J.; Park, S.B.; Choi, D.H.; Lee, S.Y.; Yoo, J.T.; Lee, S.Y. Coffee-driven green activation of cellulose and its use for all-paper flexible supercapacitors. *ACS Appl. Mater. Inter.* **2017**, *9*, 22568–22577. [CrossRef] [PubMed]
26. Si, C.; Guo, Q. Progress research on activation mechanism and regeneration of activated carbon. *China Powder Sci. Technol.* **2008**, *5*, 48–52.
27. Yang, S.; Wang, S.; Liu, X.; Li, L. Biomass derived interconnected hierarchical micro-meso-macro- porous carbon with ultrahigh capacitance for supercapacitors. *Carbon* **2019**, *147*, 540–549. [CrossRef]
28. Zhi, L.; Xu, Z.; Tan, X.; Wang, H.; Holt, C.M.B.; Stephenson, T.; Olsen, B.C.; Mitlin, D. Mesoporous nitrogen-rich carbons derived from protein for ultra-high capacity battery anodes and supercapacitors. *Energ. Environ. Sci.* **2013**, *6*, 871–878.
29. Patino, J.; Lopez-Salas, N.; Gutierrez, M.C.; Carriazo, D.; Ferrer, M.L.; Monte, F.D. Phosphorus-doped carbon-carbon nanotube hierarchical monoliths as true three-dimensional electrodes in supercapacitor cells. *J. Mater. Chem. A* **2016**, *4*, 1251–1263. [CrossRef]
30. Liu, X.; Liu, X.; Sun, B.; Zhou, H.; Li, H. Carbon materials with hierarchical porosity: Effect of template removal strategy and study on their electrochemical properties. *Carbon* **2018**, *130*, 680–691. [CrossRef]
31. Sun, B.; Yuan, Y.; Li, H.; Li, X.; Zhang, C.; Guo, F.; Liu, X.; Wang, K.; Zhao, X.S. Waste-cellulose-derived porous carbon adsorbents for methyl orange removal. *Chem. Eng. J.* **2019**, *371*, 55–63. [CrossRef]
32. Li, R.; Huang, J.; Li, W.; Li, J.; Cao, L.; Xu, Z.; He, Y.; Yu, A.; Lu, G. Controlling carbon-oxygen double bond and pseudographic structure in shaddock peel derived hard carbon for enhanced sodium storage properties. *Electrochim. Acta* **2019**, *313*, 109–115. [CrossRef]
33. Sun, Z.; Zhao, L.; Liu, C.; Zhen, Y.; Zhang, W.; Ma, J. A novel 3D adsorbent of reduced graphene oxide-β-cyclodextrin aerogel coupled hardness with softness for efficient removal of bisphenol A. *Chem. Eng. J.* **2019**, *372*, 896–904. [CrossRef]
34. Liu, J.; Wang, Z.; Wu, X.; Yuan, X.; Wu, Y. Porous carbon derived from disposable shaddock peel as an excellent catalyst toward VO2+/VO2+ couple for vanadium redox battery. *J. Power Sources* **2015**, *299*, 301–308. [CrossRef]
35. Gao, H.; Sun, Y.; Zhou, J.; Xu, R.; Duan, H. Mussel-inspired synthesis of polydopamine-functionalized graphene hydrogel as reusable adsorbents for water purification. *ACS Appl. Mater. Inter.* **2013**, *5*, 425–432. [CrossRef] [PubMed]
36. Yang, Q.; Lu, R.; Ren, S.; Chen, C.; Chen, Z. Three dimensional reduced graphene oxide/ZIF-67 aerogel: Effective removal cationic and anionic dyes from water. *Chem. Eng. J.* **2018**, *348*, 202–211. [CrossRef]
37. Dilek, A. Utilization of activated carbon produced from fruit juice industry solid waste for the adsorption of Yellow 18 from aqueous solutions. *Bioresour. Technol.* **2014**, *168*, 259–266.
38. Geng, J.; Gu, F.; Chang, J. Fabrication of magnetic lignosulfonate using ultrasonic-assisted in situ synthesis for efficient removal of Cr(VI) and Rhodamine B from wastewater. *J. Hazard. Mater.* **2019**, *375*, 174–181. [CrossRef]
39. Ai, L.; Zhang, C.; Liao, F.; Wang, Y.; Li, M.; Meng, L.; Jiang, J. Removal of methylene blue from aqueous solution with magnetite loaded multi-wall carbon nanotube: Kinetic, isotherm and mechanism analysis. *J. Hazard. Mater.* **2011**, *198*, 282–290. [CrossRef]
40. Liu, X.; Wang, Y.; Ju, H.; Yang, F.; Zhang, L.; Luo, X. Micro-mesoporous divinyl benzene-based polymer for ultrafast, effective and selective removal of cationic dyes. *Mater. Chem. Phys.* **2020**, *255*, 123564. [CrossRef]
41. Fan, L.; Luo, C.; Li, X.; Lu, F.; Qiu, H.; Sun, M. Fabrication of novel magnetic chitosan grafted with graphene oxide to enhance adsorption properties for methyl blue. *J. Hazard. Mater.* **2012**, *215–216*, 272–279. [CrossRef]
42. Liu, Q.; Yu, H.; Zeng, F.; Li, X.; Sun, J.; Li, C.; Lin, H.; Su, Z. HKUST-1 modified ultrastability cellulose/chitosan composite aerogel for highly efficient removal of methylene blue. *Carbohyd. Polym.* **2021**, *255*, 117402. [CrossRef]
43. Liang, C.; Liu, Y.; Yan, C.; Zhou, S. Green synthesis of loofah fiber-based adsorbents with high adsorption performance for methylene blue. *Mater. Lett.* **2021**, *284*, 128929. [CrossRef]
44. Peng, N.; Hu, D.; Zeng, J.; Li, Y.; Liang, L.; Chang, C. Superabsorbent cellulose–clay Nanocomposite hydrogels for highly efficient removal of dye in water. *ACS Sustain. Chem. Eng.* **2016**, *4*, 7217–7224. [CrossRef]
45. Spagnoli, A.A.; Giannakoudakis, D.A.; Bashkova, S. Adsorption of methylene blue on cashew nut shell based carbons activated with zinc chloride: The role of surface and structural parameters. *J. Mol. Liq.* **2017**, *229*, 465–471. [CrossRef]
46. Vunain, E.; Biswick, T. Adsorptive removal of methylene blue from aqueous solution on activated carbon prepared from Malawian baobab fruit shell wastes: Equilibrium, kinetics and thermodynamic studies. *Sep. Sci. Technol.* **2019**, *54*, 27–41. [CrossRef]
47. Li, Y.; Xiao, H.; Pan, Y.; Zhang, M.; Jin, Y. Thermal and pH dual-responsive cellulose microfilament spheres for dye removal in single and binary systems. *J. Hazard. Mater.* **2019**, *377*, 88–97. [CrossRef]
48. Gouthaman, A.; Asir, J.A.; Gnanaprakasam, A.; Sivakumar, V.M.; Thirumarimurugan, M.; Ahamed, M.A.R.; Azarudeen, R.S. Enhanced dye removal using polymeric nanocomposite through incorporation of Ag doped ZnO nanoparticles: Synthesis and characterization. *J. Hazard. Mater.* **2019**, *373*, 493–503.

49. Dhanavel, S.; Nivethaa, E.A.K.; Dhanapal, K.; Gupta, V.K.; Narayanan, V.; Stephen, A. α-MoO_3/polyaniline composite for effective scavenging of Rhodamine B, Congo red and textile dye effluent. *RSC Adv.* **2016**, *6*, 28871–28886. [CrossRef]
50. Ahmad, A.A.; Hameed, B.H. Fixed-bed adsorption of reactive azo dye onto granular activated carbon prepared from waste. *J. Hazard. Mater.* **2010**, *175*, 298–303. [CrossRef]
51. Shi, S.L.; Lv, J.P.; Liu, Q.; Nan, F.R.; Jiao, X.Y.; Feng, J.; Xie, S.L. Application of Phragmites australis to remove phenol from aqueous solutions by chemical activation in batch and fixed-bed columns. *Environ. Sci. Pollut. Res.* **2018**, *25*, 23917–23928. [CrossRef] [PubMed]